



PINK1-parkin pathway of mitophagy protects against contrast-induced acute kidney injury via decreasing mitochondrial ROS and NLRP3 inflammasome activation

Qisheng Lin¹, Shu Li¹, Na Jiang, Xinghua Shao, Minfang Zhang, Haijiao Jin, Zhen Zhang, Jianxiao Shen, Yijun Zhou, Wenyan Zhou, Leyi Gu, Renhua Lu, Zhaohui Ni^{*}

Department of Nephrology, Renji Hospital, School of Medicine, Shanghai Jiaotong University, Shanghai, 200127, China

ARTICLE INFO

Keywords:

Acute kidney injury
Contrast media
Mitophagy
Mitochondrial ROS
NLRP3 inflammasome
Apoptosis

ABSTRACT

Contrast-induced acute kidney injury (CI-AKI) occurs in more than 30% of patients after intravenous iodinated contrast media and causes serious complications, including renal failure and mortality. Recent research has demonstrated that routine antioxidant and alkaline therapy failed to show benefits in CI-AKI patients with high risk for renal complications. Mitophagy is a mechanism of selective autophagy, which controls mitochondrial quality and mitochondrial reactive oxygen species (ROS) through degradation of damaged mitochondria. The role of mitophagy and its regulation of apoptosis in CI-AKI are poorly understood. In this study, we demonstrated that mitophagy was induced in renal tubular epithelial cells (RTECs) during CI-AKI, both *in vivo* and *in vitro*. Meanwhile, contrast media-induced mitophagy was abolished when silencing PINK1 or PARK2 (Parkin), indicating a dominant role of the PINK1-Parkin pathway in mitophagy. Moreover, mitochondrial damage, mitochondrial ROS, RTEC apoptosis, and renal injury under contrast exposure were more severe in PINK1- or PARK2-deficient cells and mice than in wild-type groups. Functionally, PINK1-Parkin-mediated mitophagy prevented RTEC apoptosis and tissue damage in CI-AKI through reducing mitochondrial ROS and subsequent NLRP3 inflammasome activation. These results demonstrated that PINK1-Parkin-mediated mitophagy played a protective role in CI-AKI by reducing NLRP3 inflammasome activation.

1. Introduction

Contrast-induced acute kidney injury (CI-AKI) is the third most common cause of hospital-acquired acute kidney injury (AKI), occurring in more than 30% patients receiving iodinated contrast media injection, and it is associated with a high risk of mortality due to renal failure [1]. The European Society of Urogenital Radiology defined CI-AKI as an increase in serum creatinine to 44 $\mu\text{mol/L}$, 0.5 mg/dL, or of 25% from baseline within 3 days of contrast media injection, provided an alternative aetiology is excluded [2]. Recent research demonstrated that routine antioxidant and alkaline therapy showed no benefits in CI-AKI patients with high risk for renal complications [3]. The major mechanism of CI-AKI includes direct cytotoxic effects on renal tubular and vascular endothelial cells, oxidative stress, and vasoconstrictor release by iodinated contrast media [4]. Unfortunately, the exact pathogenesis of CI-AKI remains unclear, which has resulted in a lack of

effective prevention and treatment for CI-AKI.

Our previous research, as well as other investigators, proposed that activation of the nucleotide-binding oligomerisation domain-like pyrin domain containing protein 3 (NLRP3) inflammasome and release of interleukin 1 beta (IL-1 β) and IL-18 played an important role in the pathogenesis of CI-AKI and aggravation of renal function injury [5–7]. However, the mechanism of NLRP3 inflammasome activation was ill-defined in CI-AKI. Previous studies generally suggested that the activators of the NLRP3 inflammasome included pattern recognition receptor-induced nuclear factor κB (NF- κB) transcription, potassium efflux or calcium influx induced by pathogen-associated molecular patterns or damage-associated molecular patterns, reactive oxygen species (ROS) production, lysosomal rupture, and mitochondrial dysfunction [8]. Of note, mitochondrial ROS was proposed to promote deubiquitylation of NLRP3 and then activate the NLRP3 inflammasome [9].

^{*} Corresponding author. Department of Nephrology, Renji Hospital, School of Medicine, Shanghai Jiaotong University, No. 160, Pu Jian Road, Shanghai, 200127, China.

E-mail address: profnizh@126.com (Z. Ni).

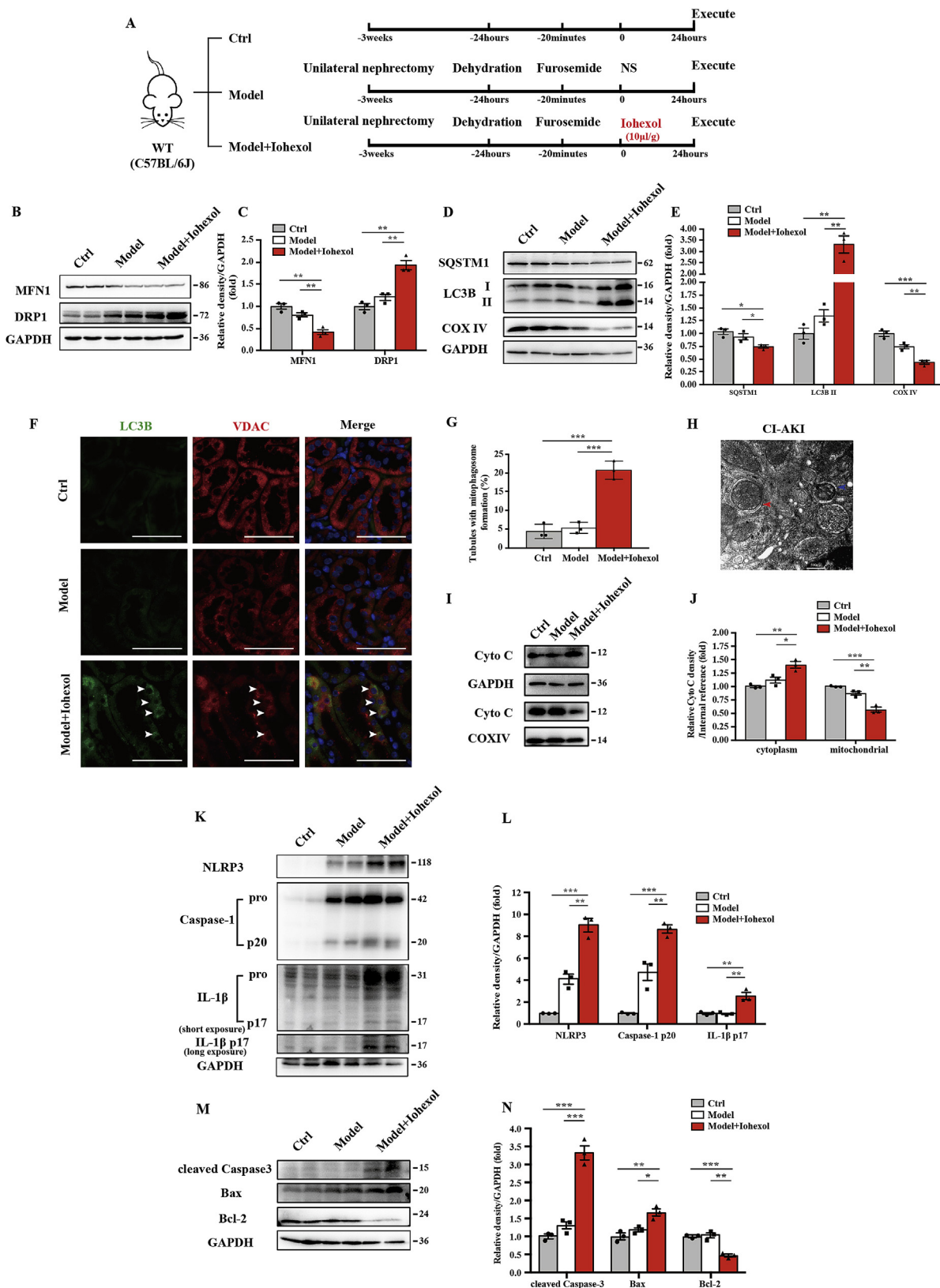
¹ These authors contributed equally to this work.

<https://doi.org/10.1016/j.redox.2019.101254>

Received 6 March 2019; Received in revised form 31 May 2019; Accepted 10 June 2019

Available online 11 June 2019

2213-2317/ © 2019 Published by Elsevier B.V. This is an open access article under the CC BY-NC-ND license (<http://creativecommons.org/licenses/by-nc-nd/4.0/>).



(caption on next page)

Recently, mitophagy has been reported to be physiologically responsible for mitochondrial quality control and mitochondrial ROS balance by removing mitochondria when damaged [10,11]. PTEN induced putative kinase 1 (PINK1)- parkin RBR E3 ubiquitin protein

ligase (Parkinson disease 2, Parkin, PARK2) mediated mitophagy is Parkin-dependent pathway of mitophagy [12]. PINK1 is a serine/threonine kinase targeting mitochondria, which has a transmembrane fragment and kinase domain in its N terminal [13,14]. In normal

Fig. 1. Mitophagy and activation of the NLRP3 inflammasome were induced in renal tubular epithelial cells in CI-AKI mice. (A) Diagrammatic representation of the inducible strategy in CI-AKI mice (Model + Iohexol, 10 μ L/g), negative control mice (Model + NS, 10 μ L/g), and control mice. (B–E) Immunoblot analysis and quantification of MFN1, DRP1, SQSTM1, LC3B I/II, and COX IV in the kidneys. (F, G) Representative images of immunofluorescence double-labelling autophagosomes (LC3B) and mitochondria outer membrane protein (VDAC) in WT mice. The percentage of renal tubules with mitophagosome formation was quantified. Scale bar: 50 μ m. (H) Representative TEM images of a mitophagosome (red arrow) and a mitophagolysosome (blue arrow) in renal tubular epithelial cells after iohexol injection. Scale bar: 500 nm. (I, J) Fresh kidneys of WT mice were fractionated to collect cytosolic and mitochondrial fraction for immunoblot analysis of cytochrome c release. (K–N) Immunoblot analysis and quantification of NLRP3, caspase-1 p20, IL-1 β p17, cleaved caspase-3, Bax, and Bcl-2 in the kidneys of WT mice. Data were presented as mean \pm TEM. n = 3–4. *p < 0.05, **p < 0.01, ***p < 0.001. (For interpretation of the references to colour in this figure legend, the reader is referred to the Web version of this article.)

mitochondria, PINK1 inserts in the mitochondrial inner membrane and intermembrane space by combining the translocator of the outer mitochondrial membrane complex and is rapidly degraded by the stromal processing peptidase. When mitochondria are injured, PINK1 accumulates in the mitochondrial outer membrane and then phosphorylates the ubiquitin and E3 ubiquitin ligase Parkin. After phosphorylation, Parkin is massively activated to ubiquitinate various mitochondrial inner proteins, which helps to recruit and activate more Parkin through positive feedback. Phosphorylated Parkin delivers ubiquitin mitochondria to developing autophagosome by combining Sequestosome1 (SQSTM1) and microtubule-associated proteins 1 light chain 3 beta (MAP1LC3B/LC3B), resulting in mitophagy and removal of damaged mitochondria through autophagy machinery [13,14]. In addition, the Parkin-independent pathway of mitophagy is mediated by Bcl-2 and adenovirus E1B 19-kDa-interacting protein3 (BNIP3) or BNIP3-like (BNIP3L), which is activated to bind directly to LC3B to promote mitophagy under hypoxia conditions [15,16].

In kidney diseases, PINK1-Parkin-mediated mitophagy is reported to play a protective role in chronic kidney disease (CKD) and AKI models [17–20]. Li and colleagues showed that PINK1-Parkin-mediated mitophagy was reduced in diabetic kidney disease (DKD), which could be rescued by Mito Q to decrease the apoptosis of renal tubular epithelial cells (RTECs) [17]. Dong's laboratory found that in renal ischemia-reperfusion injury, PINK1-Parkin-mediated mitophagy was activated to protect RTECs through reducing mitochondrial damage, ROS production, and inflammatory response [18]. The latest research demonstrated knocking out PINK1 or PARK2 caused more apoptosis, mitochondrial dysfunction, and tissue damage during cisplatin-induced nephrotoxicity, both *in vivo* and *in vitro* [19,20]. Several research studies have suggested that mitophagy was upregulated under contrast media exposure [21–23]. However, the function and regulation of PINK1-Parkin-mediated mitophagy in CI-AKI remain largely unknown. The purpose of this article is to investigate the role of the PINK1-Parkin pathway of mitophagy and its regulation on the NLRP3 inflammasome in contrast-induced apoptosis of RTECs.

2. Materials and methods

2.1. Cells, small interfering RNA, antibodies, and reagents

Human renal proximal tubular cell line (HK-2 Cell) was obtained from American Type Culture Collection (ATCC[®] CRL-2190). We obtained iohexol from GE Healthcare, mannitol (M9546) from Sigma, 3-Methyladenine (3-MA, HY-19312) from MedChemExpress (MCE), MitoTEMPO (SML0737) from Sigma and MCC950 (HY-12815) from MCE. We obtained antibodies targeting mitofusin1 (MFN1, ab57602), voltage-dependent anion channel (VDAC, ab14734), PINK1 (ab23707), 8-OHdG (ab48508) from Abcam; Dynamin-related protein 1 (DRP1, #8570), SQSTM1 (#39749), LC3B (mouse, #83506), COX IV (#4844), NLRP3 (#15101), cleaved caspase-3 (#9664), Bax (#2772), from Cell Signal Technology; LC3B (rabbit, L7543) from Sigma-Aldrich; GADPH (sc-66163), caspase-1 (sc-56036) from Santa Cruz Biotechnology; IL-1 β (Mouse, AF-401-NA; Human, AF-201-NA) from R&D Systems; MnSOD (24127-1-AP), Bcl-2 (12789-1-AP), Cyto C (10993-1-AP) from Proteintech; PINK1 (BC100-494), Parkin (NBP2-67017) from Novas Biologicals. Fluorescence secondary antibodies were obtained from

Abcam: Donkey Anti-Rabbit IgG (Alexa Fluor[®] 488, ab150073; Alexa Fluor[®] 555, ab150074), Donkey Anti-Mouse IgG (Alexa Fluor[®] 555, ab150110; Alexa Fluor[®] 488, ab150105) and Donkey Anti-Goat IgG (Alexa Fluor[®] 488, ab150129). MitoTracker Red(M7512) and MitoSOX (M36008) were obtained from ThermoFisher scientific. TUNEL assay kit (C1088) was obtained from Beyotime. The sequences of small interfering RNA (siRNA) were as follows: PINK1 siRNA 5'-GAGUAGCCG CAAAUGUGCUUCAUCU-3', PARK2 siRNA 5'-UCCA GCUCAAGGAGGU GGUUGCUAA-3'.

2.2. Animals and CI-AKI

PINK1 knockout (PINK1^{-/-}) and PARK2 knockout (PARK2^{-/-}) mice on C56BL/6J background were purchased from Jackson Laboratory, housed in pathogen-free conditions, and reproduced in Shanghai Research Center of the Southern model organisms. CI-AKI model was induced in mice as described in our recent works (Fig. 1A) [5,6]. All groups of mice were sacrificed at 24 h after iohexol/normal saline (NS) administration to harvest serum and kidney. All animal experiments were approved by the Animal Care Committee at the Renji Hospital, School of Medicine, Shanghai Jiao Tong University, and conducted following the Animal Protocol Committee of Shanghai Jiao Tong University.

2.3. Contrast media-induced HK-2 cells

HK-2 cells were cultivated in DMEM/F-12 (ThermoFisher Scientific, 11330057) with 10% foetal bovine serum (ThermoFisher Scientific, 10099158). Transient transfections of HK-2 cells with siRNA (50 nM) were performed by Lipofectamine[™] 3000 Transfection Reagent (ThermoFisher Scientific, L3000150) for 8 h. 3-MA (5 nM), MitoTEMPO (100 μ M), or MCC950 (10 μ M) was added to culture medium for 4 h before exposing to contrast media [24–26]. The method of contrast-induced HK-2 cells (20 mgI/ml) was completed as previous described [5,6], and HK-2 cells were collected for use at 72 h after incubating with iohexol. Experiments were performed in triplicate.

2.4. Renal function, histopathology, immunohistochemical and immunofluorescence staining

Serum creatinine was analysed by standard spectrophotometric assay (Roche Diagnostic GmbH). Kidney tissues were fixed with 4% paraformaldehyde (PFA), embedded 10% in paraffin, and sectioned at 4 μ m for haematoxylin and eosin (HE) staining. HE staining of kidneys was detected by microscopy, and the images were analysed by computerised digital image analysis (Ocular 2.0). The tubular injury was examined by the percentage of damaged tubules: grade 0, no damage; grade 1, < 25%; grade 2, 25–49%; grade 3, 50–75%; grade 4, > 75%.

Paraffin-embedded kidney sections (4 μ m) were deparaffinised, and ethylene diamine tetra acetic acid (1 mM) was used for antigen retrieval. Hydrogen peroxide (H₂O₂, 0.03%) was used for immunohistochemical study, and 8-OHdG (1:100) antibody was incubated overnight at 4 $^{\circ}$ C. For immunofluorescence, the slides were incubated with LC3B, Parkin, voltage-dependent anion channel (VDAC), caspase-1, or IL-1 β antibodies (1:100) at 4 $^{\circ}$ C overnight. The images were detected by fluorescence microscopy (ZEISS, Axio Vert A1), and positive

images were analysed by computerised digital image analysis. The intensity of immunofluorescence was analysed using Image J.

HK-2 cells were cultivated on cell slides for staining. For labelling mitochondria, MitoTracker Red (500 nM) was added to living HK-2 cells at 37 °C for 30 min and then fixed by 4% PFA. Then, 0.1% Triton-X-100 was used to permeate cell membrane for 5 min at room temperature. The cell slides were incubated with LC3B, PINK1, Parkin, 8-OHdG, caspase-1, or IL-1 β antibodies (1:100) at 4 °C overnight. After incubating with secondary antibody, the images were detected by confocal microscopy (ZEISS 710) or fluorescence microscopy at 550 nm for MitoTracker Red and respective wavelength for fluorescence secondary antibodies. For quantification, 10 fields were randomly selected from each group, and the amounts of positive tubules or cells per 0.25 mm² were evaluated.

2.5. Transmission electron microscopy

Fresh kidneys and HK-2 cells were harvested in 1 mm³, prefixed in 2% glutaraldehyde, and fixed in 1% osmium tetroxide. Next, samples were dehydrated in ethanol with 3% uranyl acetate, embedded in the epoxy resin and propylene oxide overnight, and polymerised. After slicing into 70-nm-thick sections and staining with lead citrate, the sections were detected by H-7650 transmission electron microscope (Hitachi H-7650). Two blinded pathologists were invited independently to quantify each section.

2.6. Mitochondrial isolation

Tissue and cell mitochondrial extraction kits (Beyotime, C3606, C3601) were used for mitochondrial isolation of kidney and HK-2 cells according to the manufacturer's instructions. The mitochondria and cytoplasm were isolated through differential centrifugation and kept in a storage solution with phenylmethylsulfonyl fluoride for immunoblot analysis.

2.7. Quantification of mitochondrial DNA

Kidneys were harvested to isolate total DNA by using the DNeasy Blood and Tissue kit (Qiagen, 69504) according to the manufacturer's instructions. Quantification of mitochondrial DNA (mtDNA) was detected by mitochondrial NADH-ubiquinone oxidoreductase chain 1 (MT-ND1) and nuclear DNA (nDNA) named beta-2 microglobulin (B2M). Mouse primers were purchased from Takara: MT-ND1 forward, 5'-TCTAATCGCCATAGCCTTC-3'; reverse, 5'-GCGTCTGCAAAT GGT TGTA-3'; B2M forward, 5'-ACGTAACACAGTCCACCCG-3'; reverse, 5'-CGGCCATACT GGCATGCTTA -3'.

2.8. Analysis of mitochondrial ROS

Mitochondrial ROS activity was detected by the MnSOD Assay Kit with WST-8 (Beyotime, S0103) according to the manufacturer's instructions. The enzymatic activity of MnSOD was adjusted by protein concentration.

MitoSOX was also used to detect the mitochondrial ROS level in living HK-2 cells. Cells were incubated in MitoSOX (5 μ M) and Hoechst (5 μ g/ml, MedChemExpress, HY-15631) for 30 min at 37 °C, and positive staining was subsequently detected by fluorescence microscopy for image or detected by BioTak CytationTM³ for quantification of relative fluorescence units (RFU) at 550 nm.

2.9. Real-time polymerase chain reaction

The kidney injury was also measured by gene expression of kidney injury molecule-1 (KIM-1) assessed by quantitative real-time polymerase chain reaction. Mouse KIM-1 primers were purchased from Takara: forward, 5'-CCTTGAGACCGTGCTA-3'; reverse, 5'-TGTT

GTCTTC AGCTCGGGAATG-3'.

2.10. Immunoblot analysis

For immunoblot analysis, the protein from kidney and HK-2 cells was separated in 8%, 10%, or 12% sodium dodecyl sulphate polyacrylamide gel electrophoresis, and polyvinylidene difluoride membranes were incubated in primary antibodies at 4 °C overnight. Image J software was used for densitometry analysis, and the data were normalised against glyceraldehyde-3-phosphate dehydrogenase.

2.11. Analysis of apoptosis

Apoptosis was measured by terminal deoxynucleotidyl transferase (TdT) dUTP nick-end labelling (TUNEL) staining, flow cytometry, and immunoblot analysis of cleaved caspase-3, Bax, and Bcl-2. TUNEL staining was detected by TdT enzyme according to the manufacturer's instructions, and TUNEL-positive cells were calculated per 0.25 mm². Flow cytometry was performed by labelling Annexin V and propidium iodide according to manufacturer's instructions (BD Biosciences, 556547). Flow cytometry was tested by BD LSR Fortessa, and data were analysed by FlowJO software.

2.12. Statistics

Statistical analysis was performed using Prism 6 (GraphPad). Qualitative data were expressed as means \pm standard error of the mean (SEM) and analysed by two-tailed unpaired Student's *t*-test between two groups or one-way analysis of variance followed by Tukey's post-tests between multiple groups. *P* < 0.05 was considered significant.

3. Results

3.1. Mitophagy and activation of the NLRP3 inflammasome were induced in RTECs in CI-AKI mice

To investigate mitophagy and its effect on the NLRP3 inflammasome in CI-AKI, we first established a CI-AKI mice model with the low-osmolar nonionic monomer iohexol as described before [5,6] (Fig. 1A). Iohexol injection by tail vein decreased MFN1 and increased DRP1, which suggested that mitochondrial dynamics change in CI-AKI with less fusion and more fission (Fig. 1B and C). Next, immunoblot analysis of autophagy biomarkers, SQSTM1 and LC3B, showed that autophagy was activated and mitochondrial inner membranous protein COX IV was reduced in the CI-AKI groups (Fig. 1D and E). Further immunofluorescence staining of LC3B and VDAC, a mitochondrial outer membranous protein, revealed increased mitophagy in RTECs in CI-AKI mice (Fig. 1F and G). Meanwhile, both stages of mitophagy, mitophagosome and mitophagolysosome formation, were found in RTECs in CI-AKI (Fig. 1H). After iohexol injection, more cytochrome C was released from mitochondria to cytoplasm in CI-AKI than in the other two groups, suggesting that mitochondrial damage was aggravated by contrast media (Fig. 1I and J). Immunoblot analysis showed that MnSOD, SOD from mitochondria, was reduced by iohexol injection (Fig. Supplemental Figure 1). The activation of the NLRP3 inflammasome was measured using the protein level of NLRP3, cleaved caspase-1, and mature IL-1 β in kidneys, which showed little change in the model group but was significantly upregulated in the CI-AKI group (Fig. 1K and L). Proapoptotic protein, cleaved caspase-3 and Bax, was increased after iohexol injection, with decreased Bcl-2, anti-apoptotic protein (Fig. 1M and N). These data elucidated that mitophagy was activated in CI-AKI *in vivo* as well as showed NLRP3 inflammation activation and apoptosis of RTECs.

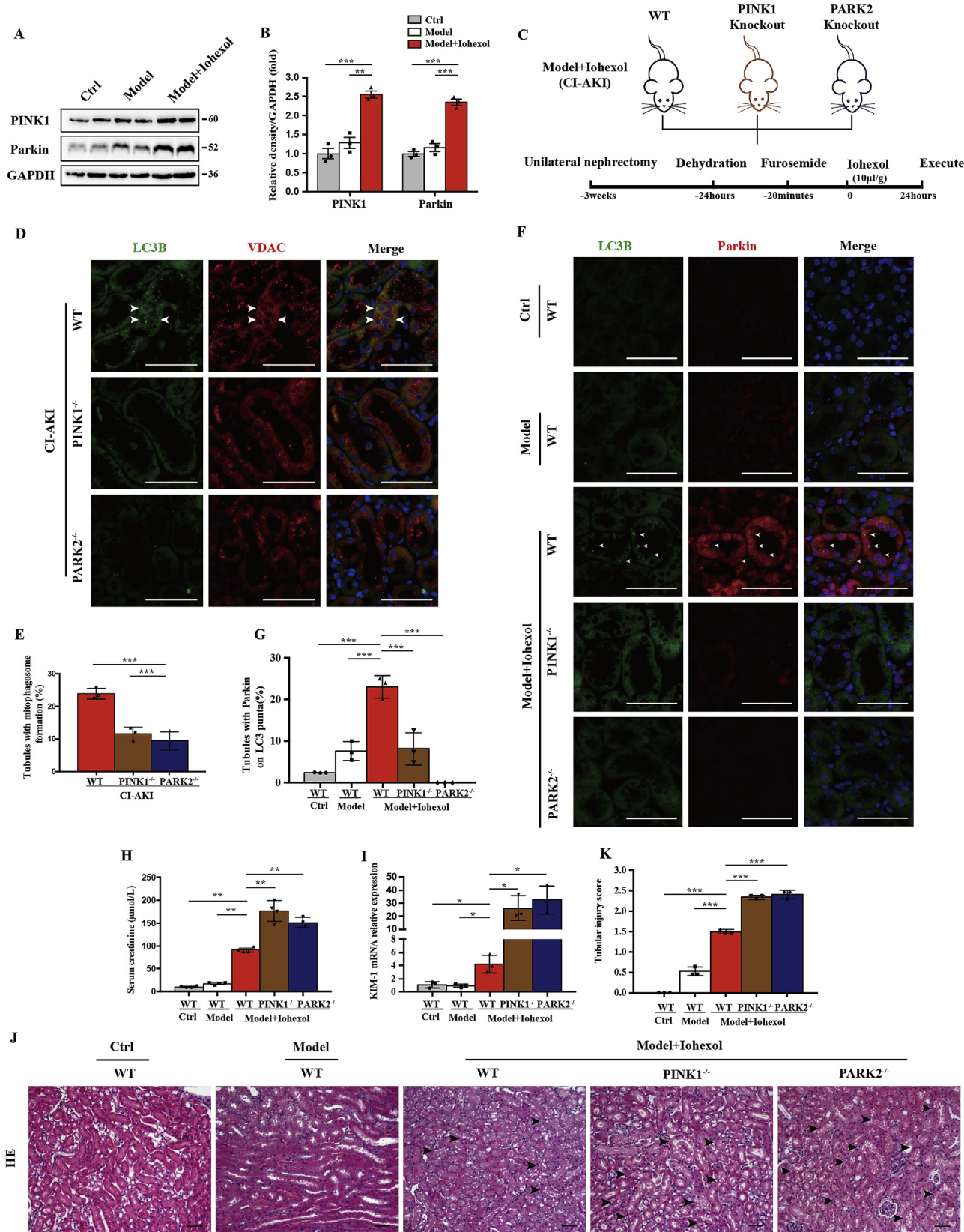


Fig. 2. PINK1 and Parkin mediated mitophagy and protected the aggravation of renal injury in CI-AKI mice. (A, B) Immunoblot analysis and quantification of PINK1 and Parkin in the kidneys. (C) Diagrammatic representation of CI-AKI in different groups of mice: WT, PINK1 knockout and PARK2 knockout. (D, E) Representative images and quantification of immunofluorescence double-labelling LC3B and VDAC in different groups of CI-AKI mice. Scale bar:50 μm. (F, G) PINK1-Parkin mediated mitophagy was showed by immunofluorescence and quantification of double-labelling LC3B and Parkin. Scale bar:50 μm. (H, I) Kidney injury was also measured by serum creatinine and kidney KIM-1 mRNA level of different groups of mice. (J, K) Representative histology and pathological score of tubular damage in kidney cortex by H-E staining. The tubular injury was indicated by arrows. Scale bar:50 μm. Data were presented as mean ± TEM. n = 3–4. *p < 0.05, **p < 0.01, ***p < 0.001. (For interpretation of the references to colour in this figure legend, the reader is referred to the Web version of this article.)

3.2. PINK1 and Parkin mediated mitophagy and protected the aggravation of renal injury in CI-AKI mice

After iohexol injection by tail vein, the mice kidney cortex showed increases in PINK1 and Parkin expression (Fig. 2A and B). To elucidate the PINK1-Parkin pathway of mitophagy in CI-AKI, we introduced PINK1^{-/-} and PARK2^{-/-} mice as the Model + Iohexol (CI-AKI) group (Fig. 2C, Fig. Supplemental Figure 2). Mitophagy was detected by co-staining of LC3B and VDAC, which decreased in RTECs in PINK1^{-/-} and PARK2^{-/-} mice (Fig. 2D and E). Immunofluorescence showed more expression of Parkin in wild-type (WT) CI-AKI groups than in the model or Ctrl groups but little expression in the PINK1^{-/-} CI-AKI group. Parkin-mediated mitophagy, assessed by co-staining of Parkin and LC3B, was upregulated in WT mice after iohexol treatment compared with the model and Ctrl groups but not in PINK1^{-/-} and PARK2^{-/-} mice with CI-AKI (Fig. 2F and G). Collectively, PINK1-PARK2-mediated mitophagy participated in CI-AKI. To further clarify the role and regulation of PINK1-Parkin-mediated mitophagy in CI-AKI, we detected serum creatinine, local KIM-1 mRNA expression, and microscopic pathology of the kidney cortex with HE staining. The average serum creatinine level was as high as 91.0 μmol/L at 24 h after iohexol injection in the WT CI-AKI group, compared with 17.5 μmol/L in the model group and 10.3 μmol/L in the Ctrl group. PINK1^{-/-} and PARK2^{-/-} CI-AKI mice showed a remarkable increase in serum creatinine to 176.3 μmol/L and 150.0 μmol/L, respectively (Fig. 2H). KIM-1 mRNA expression in the kidney cortex increased 4.3-fold in the WT CI-AKI group, 26.1-fold in the PINK1^{-/-} CI-AKI group, and 32.5-fold in the PARK2^{-/-} CI-AKI group compared with the Ctrl group (Fig. 2I). HE staining of the cortex showed kidney injury with intraepithelial vacuolar degeneration and interstitial inflammation after iohexol injection (Fig. 2J). Quantitative analysis of the tubular injury score of PINK1^{-/-} and PARK2^{-/-} CI-AKI renal tissues was 2.3 and 2.4, compared with 1.4 for WT CI-AKI kidneys (Fig. 2K). These data demonstrated that PINK1-PARK2-mediated mitophagy was activated to protect RTECs from injury in CI-AKI.

3.3. PINK1 or PARK2 deficiency enhanced contrast-induced mitochondrial ROS production and NLRP3 inflammasome activation in RTECs in vivo

Next, we examined mitochondrial morphology and mitochondrial ROS production in PINK1^{-/-} and PARK2^{-/-} mice. After Iohexol injection, mitochondrial swelling and loss of mitochondrial cristae occurred in RTECs in WT mice, which were more prominent in PINK1^{-/-} and PARK2^{-/-} mice with vacuoles formation in the matrix under transmission electron microscopy (TEM) (Fig. 3A and B). Immunoblot analysis showed mitochondrial damage aggravated in PINK1^{-/-} or PARK2^{-/-} mice, through detecting cytosolic cytochrome C released from mitochondria (Fig. 3C and D). Quantitative analysis of mitochondrial genomic DNA showed the ratio of mtDNA: nDNA was reduced in CI-AKI group compared to Ctrl group, which might be caused by mitophagy (Fig. 3E). Immunoblot analysis and quantification of MnSOD in kidney cortex of CI-AKI groups showed decreased MnSOD in PINK1^{-/-} or PARK2^{-/-} CI-AKI group compared to WT CI-AKI group (Fig. Supplemental Figure 3). The activity of MnSOD decreased after Iohexol injection and was further reduced in PINK1^{-/-} or PARK2^{-/-} group (Fig. 3F). 8-OHdG, one of the predominant forms of DNA oxidative damage, deposited in nuclear and cytoplasm increased after Iohexol injection, which was more significant in PINK1^{-/-} or PARK2^{-/-} CI-AKI group (Fig. 3G and H). Overall, these data demonstrated that mitochondrial injury and mitochondrial ROS production were worsened in PINK1^{-/-} or PARK2^{-/-} mice due to Iohexol injection, indicating PINK1-Parkin mediated mitophagy protected RTECs through decreasing mitochondrial ROS.

Immunoblot analysis of NLRP3 inflammasome showed that deficiency of PINK1 or PARK2 increased NLRP3 inflammasome activation, demonstrated by increased NLRP3, cleaved caspase-1 and mature IL-1β

(Fig. 3I and J). This was further confirmed by more production of caspase-1 or IL-1β in RTECs in PINK1^{-/-} or PARK2^{-/-} CI-AKI mice than WT CI-AKI mice shown in immunofluorescence (Fig. 3K, L). These results demonstrated that the protective effect of PINK1-Parkin mediated mitophagy for RTECs was associated with inhibiting NLRP3 inflammasome.

3.4. PINK1 or PARK2 deficiency increased apoptosis of RTECs in CI-AKI mice

We further evaluated apoptosis of RTECs in CI-AKI with or without PINK1/PARK2. Immunoblot analysis showed that the kidney cortex of PINK1^{-/-} or PARK2^{-/-} CI-AKI mice had a higher level of proapoptotic protein, namely, cleaved caspase-3 and Bax, and lower expression of anti-apoptotic protein Bcl-2 than that of WT CI-AKI mice (Fig. 4A and B). Consistent with the results of the immunoblot, TUNEL assay also revealed more apoptotic RTECs in PINK1^{-/-} or PARK2^{-/-} mice than in WT mice after iohexol injection (Fig. 4C and D).

These findings *in vivo* elucidated that PINK1-Parkin-mediated mitophagy protected RTECs through decreasing mitochondrial ROS production, inhibiting the NLRP3 inflammasome, and reducing apoptosis of RTECs after iohexol injection.

3.5. Contrast media induced PINK1-Parkin-mediated mitophagy, NLRP3 inflammasome activation, and apoptosis in HK-2 cells

In vitro, we initially cultured HK-2 cells for 72 h with iohexol (20 mg/ml) as described previously [5,6]. Iohexol-induced mitochondrial dynamics change with less fusion and more fission (Fig. 5A and B). To examine the occurrence of mitophagy in HK-2 cells, confocal microscopy revealed that the Ctrl and Mannitol group had few positive stainings of autophagosome marker LC3B, but a large number of LC3B was shown in the Iohexol group. With further co-staining with MitoTracker, a mitochondrial marker, we observed co-localised LC3B and MitoTracker in iohexol-treated HK-2 cells, indicating the formation of mitophagosomes induced by iohexol (Fig. 5C and D). Consistent with immunofluorescence, TEM also showed more mitophagosomes in iohexol-treated HK-2 cells (Fig. 5E and F). Immunoblot analysis of SQSTM1, LC3B, and COX IV revealed more autophagy activation and more mitochondrial clearance (Fig. 5G and H). In response to iohexol, HK-2 cells had an increase in PINK1 and Parkin protein expression as well as their co-localisation with MitoTracker in immunofluorescence staining (Fig. 5G–J). After iohexol treatment, mitochondrial ROS upregulated at 24 h and increased continuously over time (Fig. Supplemental Figure 4). Meanwhile, MnSOD in HK-2 cells was decreased after treatment with iohexol (Fig. Supplemental Figure 5). Both NLRP3 inflammasome activation and apoptosis of HK-2 cells were verified by immunoblot analysis, as the protein levels of NLRP3, cleaved caspase-1, mature IL-1β, cleaved caspase-3 and Bax were upregulated by contrast media, while anti-apoptotic protein Bcl-2 expression was reduced (Fig. 5M–P). Accordingly, iohexol activated PINK1-Parkin-mediated mitophagy and the NLRP3 inflammasome and induced apoptosis of HK-2 cells.

3.6. NLRP3 inflammasome and apoptosis increased in 3-MA-pretreated HK-2 cells in response to contrast media through inhibiting mitophagy

To discuss the role and regulation of mitophagy on the NLRP3 inflammasome and apoptosis, we incubated HK-2 cells with 3-MA (5 nM) for 4 h before exposure to iohexol. First, immunoblot analysis of PINK1, Parkin, SQSTM1, LC3B, and COX IV showed that mitophagy was inhibited by 3-MA (Fig. 6A and B). 3-MA-pretreated HK-2 cells showed less MnSOD expression but more activation of the NLRP3 inflammasome under contrast media intervention (Fig. 6C–F). Apoptosis was measured by proapoptosis-associated protein level and TUNEL staining. In contrast-induced HK-2 cells, cleaved caspase-3 and Bax were further

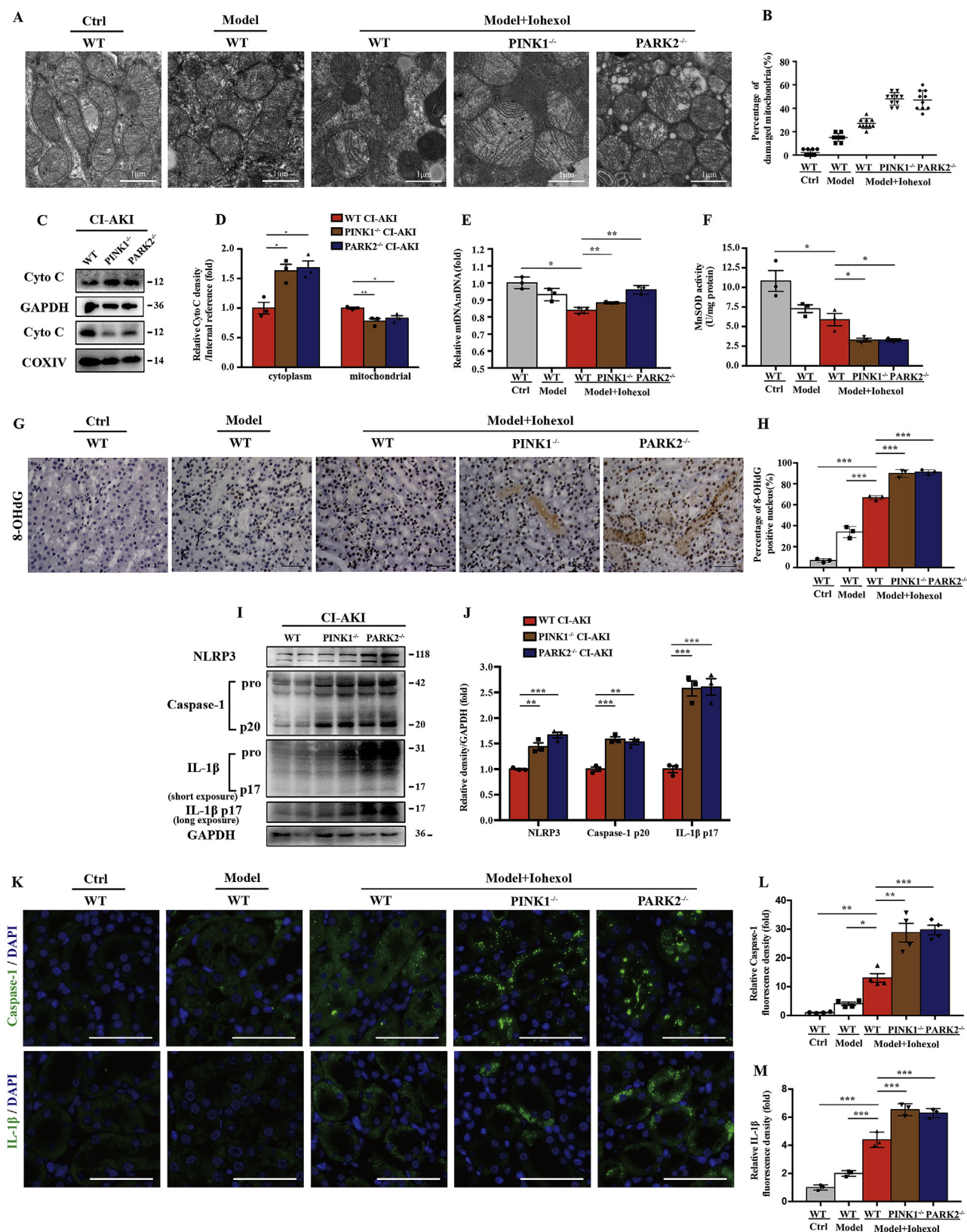


Fig. 3. PINK1 or PARK2 deficiency enhanced contrast-induced mitochondrial ROS production and NLRP3 inflammasome activation in renal tubular epithelial cells *in vivo*. (A, B) Representative TEM images of mitochondrial morphology in renal tubular epithelial cells. Data were shown as a dot plot of the percentage of damaged mitochondria from 10 images of each group. Scale bar: 1 μm. (C, D) Fresh kidneys of different groups of CI-AKI mice were fractionated to collect cytosolic and mitochondrial fraction for immunoblot analysis of cytochrome c release. (E) Relative mitochondrial DNA content (mtDNA: nDNA) of kidneys. (F) Mitochondrial ROS is assessed by MnsOD activity of fresh kidneys. (G, H) Representative images and quantification of 8-OHdG staining in kidney cortex. Scale bar: 50 μm. (I, J) Immunoblot analysis and quantification of NLRP3, caspase-1 p20, and IL-1β p17 in the kidneys of different groups of CI-AKI mice. (K–M) Representative images and quantification of immunofluorescence staining of caspase-1 and IL-1β in kidney tubules. Scale bar: 50 μm. Data were presented as mean ± TEM. n = 3. *p < 0.05, **p < 0.01, ***p < 0.001. (For interpretation of the references to colour in this figure legend, the reader is referred to the Web version of this article.)

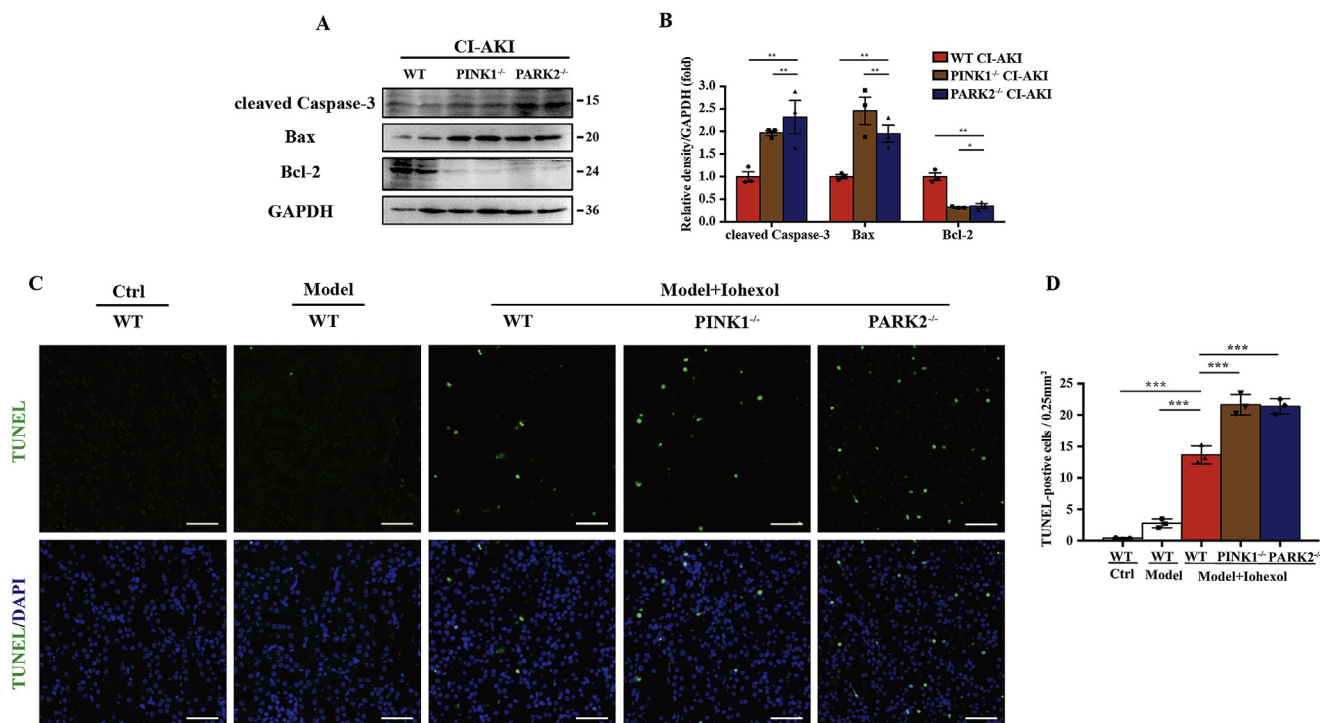


Fig. 4. PINK1 or PARK2 deficiency increased apoptosis of renal tubular epithelial cells in CI-AKI mice. (A, B) Immunoblot analysis and quantification of cleaved caspase-3, Bax, and Bcl-2 in the kidneys of different CI-AKI mice. (C, D) Apoptosis was accessed by TUNEL staining of kidney cortex and quantification of TUNEL-positive cells. Scale bar: 50 μ m. Data were presented as mean \pm TEM. n = 3. *p < 0.05, **p < 0.01, ***p < 0.001. (For interpretation of the references to colour in this figure legend, the reader is referred to the Web version of this article.)

upregulated and Bcl-2 downregulated by 3-MA pretreatment (Fig. 6G and H). Similarly, TUNEL-positive HK-2 cells increased substantially in the 3-MA-pretreated group compared with the iohexol group without 3-MA (Fig. 6I and J). These data suggested that inhibiting mitophagy with 3-MA exacerbated the NLRP3 inflammasome and apoptosis of HK-2 cells under contrast media.

3.7. Silencing PINK1 or PARK2 decreased mitophagy in contrast-treated HK-2 cells

To identify the role and function of the PINK1-PARK2 pathway of mitophagy in contrast-treated HK-2 cells, siRNA was used for silencing PINK1 or PARK2. Immunoblot analysis showed reduced autophagy activation by SQSTM1 and LC3B II and decreased mitochondrial clearance by COX IV after silencing PINK1 or PARK2 (Fig. 7A and B). Furthermore, mitophagy was detected by immunofluorescence staining. Co-localisation of LC3B and MitoTracker showed reduced formation of mitophagosomes after silencing PINK1 or PARK2 (Fig. 7C and D). Next, to verify contrast-induced Parkin-mediated mitophagy, we used double staining of LC3B and Parkin in HK-2 cells treated with iohexol. As shown in Fig. 7E and F, a large number of LC3B-labelled autophagosomes were co-localised with Parkin in the SiNC + Iohexol group but few in the SiPINK1 + Iohexol and SiPARK2 + Iohexol groups, indicating that Parkin-mediated mitophagy was activated by iohexol intervention and reduced after silencing PINK1 or PARK2 (Fig. 7E and F).

3.8. Silencing PINK1 or PARK2 increased mitochondrial ROS production and subsequently activated NLRP3 inflammasome in contrast-treated HK-2 cells

To clarify the regulatory effect of PINK1-Parkin-mediated mitophagy on mitochondrial ROS, HK-2 cells treated with contrast media were incubated in MitoSOX to label mitochondrial superoxide. As shown in Fig. 8A and B, iohexol caused an increase in mitochondrial

ROS compared with the Ctrl and Mannitol groups, and a more significant increase was observed after silencing PINK1 or PARK2. Next, we examined the quantity and activity of MnSOD. Immunoblot analysis showed that MnSOD was further decreased by silencing PINK1 or PARK2 after iohexol treatment (Fig. Supplemental Figure 6). The activity of the SOD enzyme from mitochondria decreased after iohexol intervention and was more remarkably reduced after inhibiting the PINK1-Parkin pathway of mitophagy (Fig. 8D). Next, immunofluorescence of 8-OHdG showed that mitochondrial ROS-induced DNA oxidative damage was increased by iohexol and exacerbated significantly after silencing PINK1 or PARK2 (Fig. 8A and C). Furthermore, we examined NLRP3 inflammasome activation using immunoblot analysis and immunofluorescence. Immunoblot analysis showed that NLRP3, cleaved caspase-1, and mature IL-1 β were increased with contrast media exposure after silencing PINK1 or PARK2 (Fig. 8E and F). Immunofluorescence of caspase-1 and IL-1 β demonstrated significant NLRP3 inflammasome activation in HK-2 cells treated with iohexol compared with the Ctrl and Mannitol groups. Similarly, more positive staining of caspase-1 and IL-1 β in the cytoplasm of HK-2 cells with contrast media exposure after silencing PINK1 or PARK2 indicated more NLRP3 inflammasome activation when the PINK1-Parkin pathway of mitophagy was inhibited (Fig. 8G and H). Collectively, mitochondrial ROS and NLRP3 inflammasome activation were increased by reducing PINK1-Parkin-mediated mitophagy.

However, whether mitochondrial ROS is the trigger of the NLRP3 inflammasome in iohexol-treated HK-2 cells after silencing PINK1 or PARK2 is unclear. We pretreated HK-2 cells for 4 h with 100 μ M of MitoTEMPO. MitoTEMPO-treated HK2 cells after transfection with PINK1 or PARK2 siRNA showed reduced mitochondrial ROS production under iohexol exposure (Fig. 8A and B). Other researchers have demonstrated that ROS directly induced DNA oxidative damage [27–29], and we also found using immunofluorescence that 8-OHdG had the same trend as mitochondrial ROS (Fig. 8A and C). Both immunoblot of NLRP3 inflammasome and immunofluorescence of caspase-1 and IL-1 β

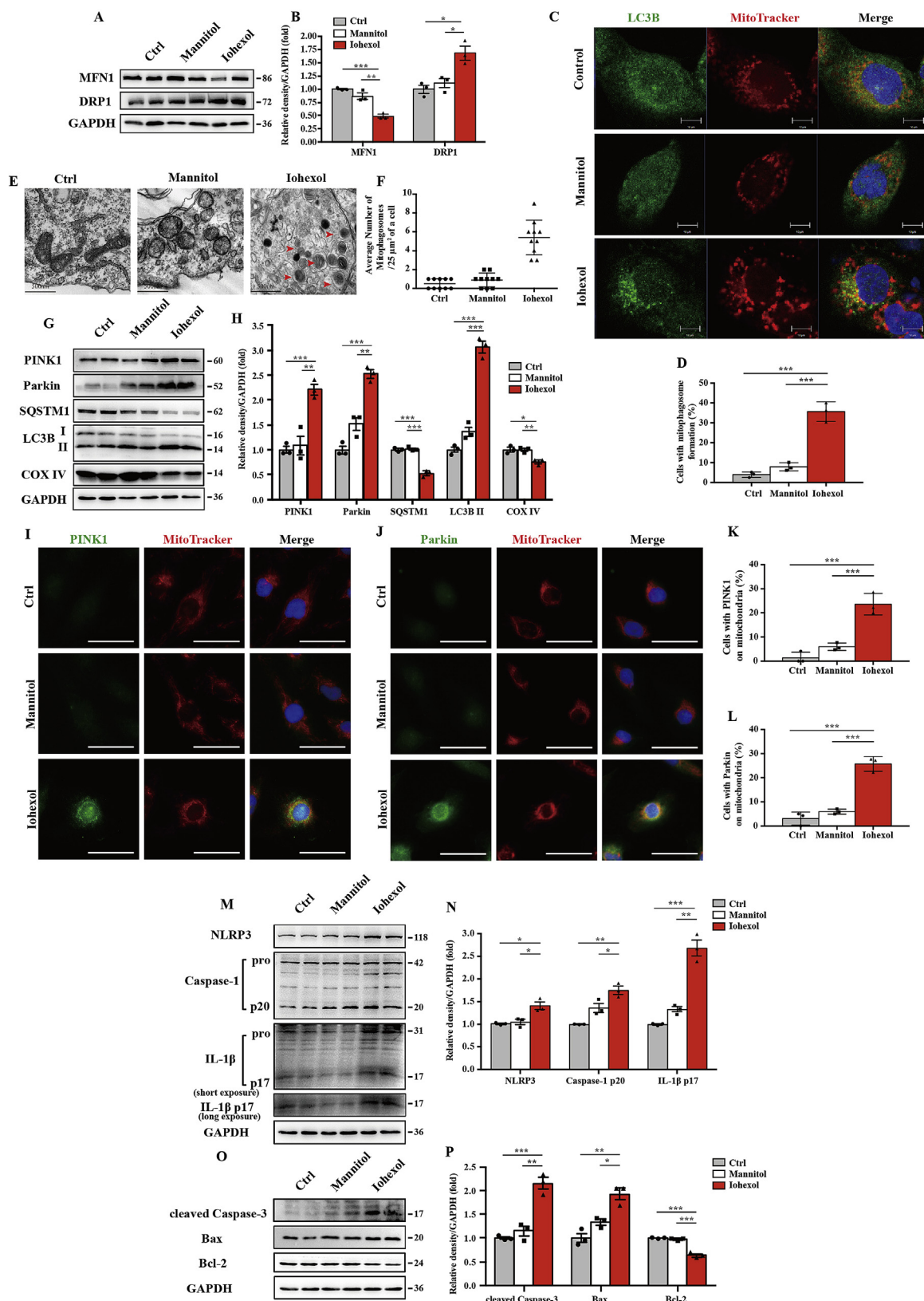


Fig. 5. Contrast media induced PINK1-Parkin-mediated mitophagy, NLRP3 inflammasome activation, and apoptosis in HK-2 cells. HK-2 cells are incubated in DMEM/F12 containing iohexol (20 mg I/ml) for 72 h. (A, B) Immunoblot analysis and quantification of MFN1 and DRP1. (C, D) Representative images and quantification of immunofluorescence double-labelling LC3B and mitochondrial marker (MitoTracker). Scale bar: 10 μm. (E, F) Representative TEM images of mitochondrial morphology and mitophagosomes (red arrow). Data were shown as a dot plot of the number of mitophagosomes from 10 images of each group. Scale bar: 500 nm. (G, H) Immunoblot analysis of PINK, Parkin, SQSTM1, LC3B I/II, and COX IV. (I–L) Representative images and quantification of immunofluorescence double-labelling PINK1/Parkin and MitoTracker. (M–P) Immunoblot analysis and quantification of NLRP3, caspase-1 p20, IL-1β p17, cleaved caspase-3, Bax, and Bcl-2. Data were presented as mean ± TEM. *p < 0.05, **p < 0.01, ***p < 0.001. (For interpretation of the references to colour in this figure legend, the reader is referred to the Web version of this article.)

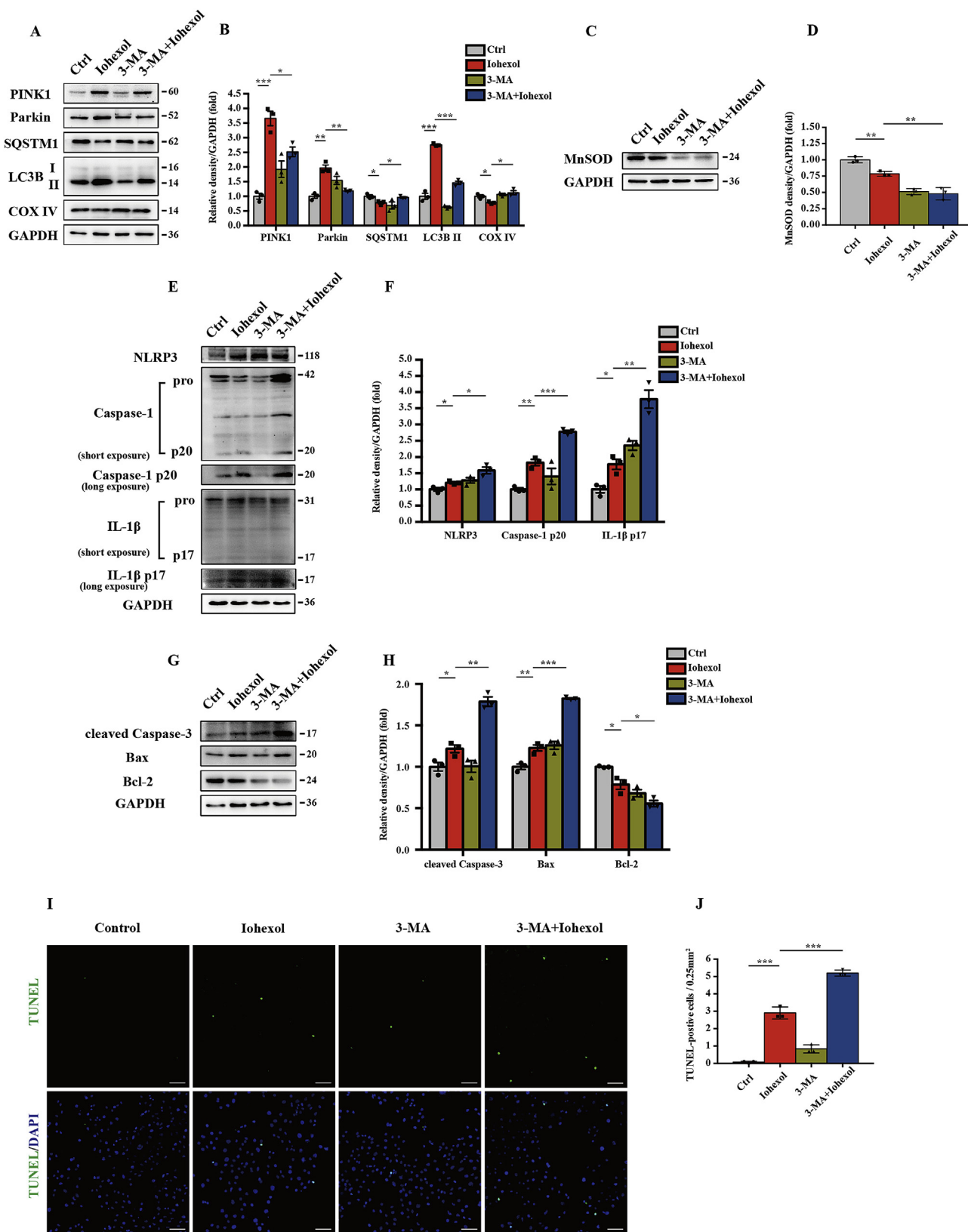


Fig. 6. NLR3 inflammasome and apoptosis increased in 3-MA-pretreated HK-2 cells in response to contrast media through inhibiting mitophagy. HK-2 cells are pretreated in 3-MA (5 nM) for 4 h and then incubated with iohexol (20 mg I/ml) for 72 h. (A, B) Immunoblot analysis and quantification of PINK1, Parkin, SQSTM1, LC3B I/II, and COX IV. (C–H) Immunoblot analysis and quantification of MnSOD, NLR3, caspase-1 p20, IL-1β p17, cleaved caspase-3, Bax, and Bcl-2. (I, J) Representative images and quantification of TUNEL staining of HK-2 cells pretreated in 3-MA. Scale bar: 100 μm. Data were presented as mean ± TEM. *p < 0.05, **p < 0.01, ***p < 0.001. (For interpretation of the references to colour in this figure legend, the reader is referred to the Web version of this article.)

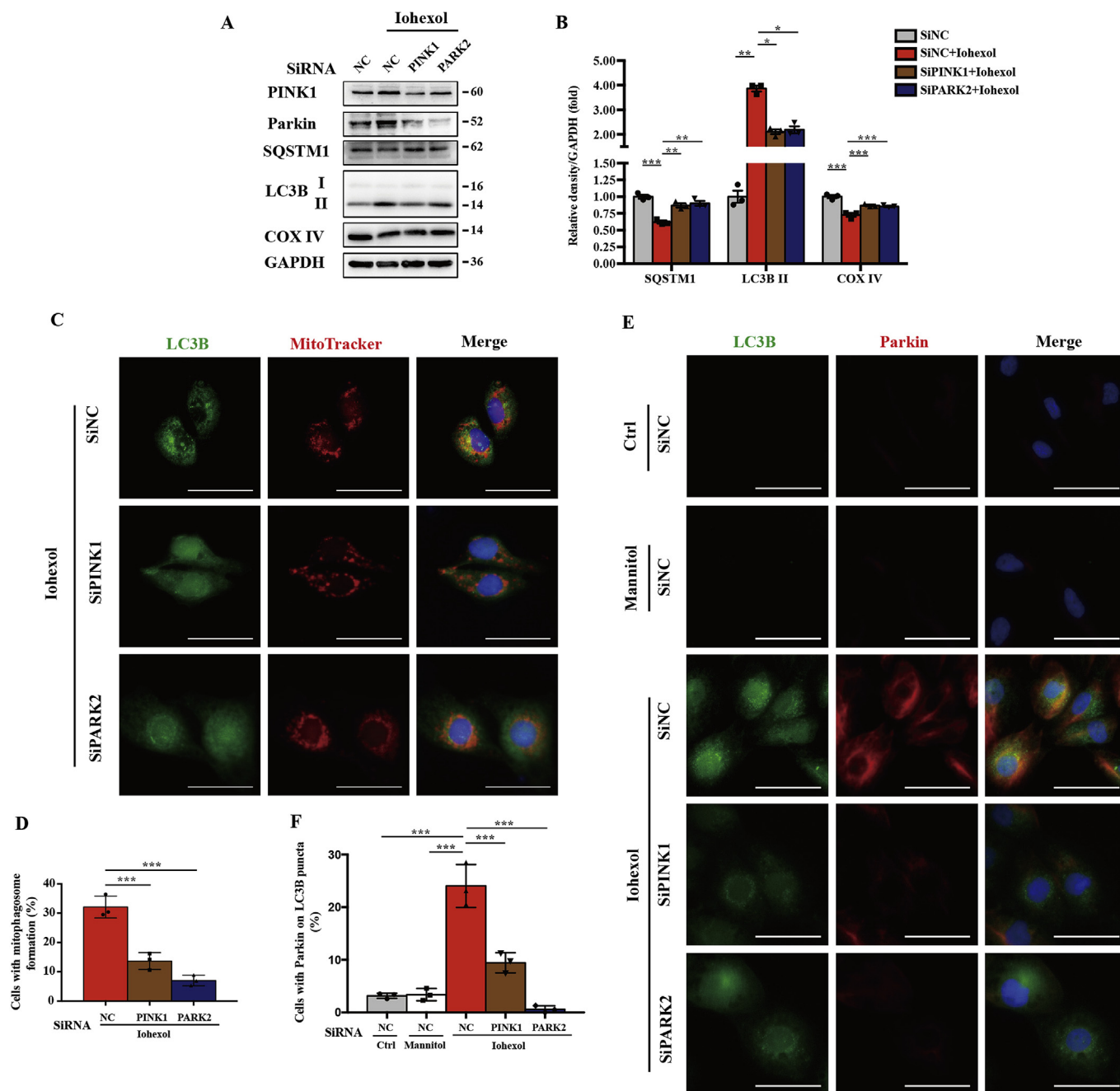


Fig. 7. Silencing PINK1 or PARK2 decreased mitophagy in contrast-treated HK-2 cells. HK-2 cells are subjected to iohexol (20 mg l/ml) for 72 h at 24 h after transfection with negative control siRNA (SiNC), PINK1 siRNA (SiPINK1), or PARK2 siRNA (SiPARK2). (A, B) Immunoblot analysis of PINK1, Parkin, SQSTM1, LC3B I/II, and COX IV. (C, D) Representative images and quantification of immunofluorescence double-labelling LC3B and MitoTracker in SiNC, SiPINK1, or SiPARK2 cells treated with iohexol. Scale bar: 50 μ m. (E, F) Representative images and quantification of double-labelling LC3B and Parkin. Scale bar: 50 μ m. Data were presented as mean \pm TEM. * p < 0.05, ** p < 0.01, *** p < 0.001. (For interpretation of the references to colour in this figure legend, the reader is referred to the Web version of this article.)

showed that overactivation of the NLRP3 inflammasome by reducing PINK1-Parkin-mediated mitophagy could be salvaged by MitoTEMPO (Fig. 8G–J). These data demonstrated that mitochondrial ROS was increased when PINK1-Parkin-mediated mitophagy was decreased, causing DNA oxidative injury and NLRP3 inflammasome activation.

3.9. Silencing PINK1 or PARK2 sensitised HK-2 cells to contrast-induced apoptosis, which was reduced by NLRP3 inflammasome inhibition

In this study, we investigated the regulatory role of PINK1-Parkin-mediated mitophagy in apoptosis. Immunoblot analysis showed

an increase of proapoptotic protein and decrease of antiapoptotic protein with iohexol exposure after silencing PINK1 or PARK2 (Fig. 9A and B). Both flow cytometry and TUNEL assay demonstrated that Annexin V-positive and TUNEL-positive HK-2 cells were increased after iohexol intervention, and more significantly after silencing PINK1 or PARK2 (Fig. 9E–G). After transfection with SiPINK1 or SiPARK2, MCC950 (10 μ M) was used to pretreat HK-2 cells before exposure to iohexol to inhibit NLRP3 inflammasome activation and explore the relationship between NLRP3 inflammasome and contrast-induced apoptosis. The apoptosis induced by iohexol after silencing PINK1 or PARK2 was abolished by MCC950, demonstrated by immunoblot analysis of

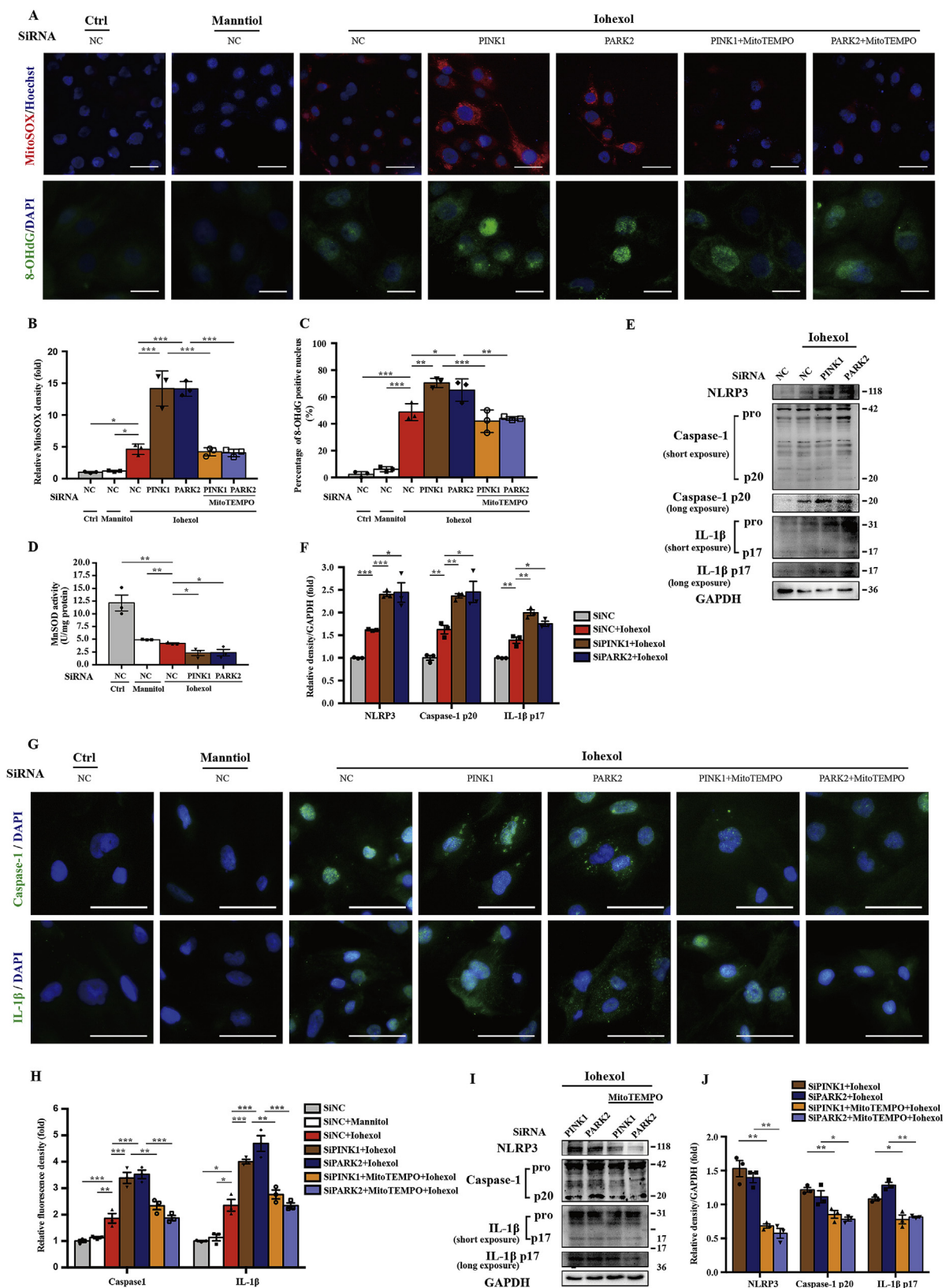


Fig. 8. Silencing PINK1 or PARK2 increased mitochondrial ROS production and subsequently activated the NLRP3 inflammasome in contrast-treated HK-2 cells. HK-2 cells were transfected with negative control siRNA, PINK1 siRNA, or PARK2 siRNA. After transfection for 8 h, cells were pretreated with MitoTEMPO (100 μM) for 4 h and then cultured with iohexol for 72 h. (A–C) Representative images and quantification of mitochondrial ROS (MitoSOX) and 8-OHdG in HK-2 cells. Scale bar: 50 μm (MitoSOX) and 25 μm (8-OHdG). (D) Mitochondrial ROS was also assessed by MnSOD activity (U/mg protein) of HK-2 cells. (E, F) Immunoblot analysis and quantification of NLRP3, caspase-1 p20, and IL-1β p17 in SINC, SiPINK1, and SiPARK2 cells with iohexol. (G, H). Representative images and quantification of immunofluorescence staining caspase-1 and IL-1β in HK-2 cells. Scale bar: 50 μm. (I–J) Immunoblot analysis and quantification of NLRP3, caspase-1 p20, and IL-1β p17 in HK-2 cells pretreated with or without MitoTEMPO, after silencing PINK1 or PARK2 in response to iohexol. Data were presented as mean ± TEM. *p < 0.05, **p < 0.01, ***p < 0.001. (For interpretation of the references to colour in this figure legend, the reader is referred to the Web version of this article.)

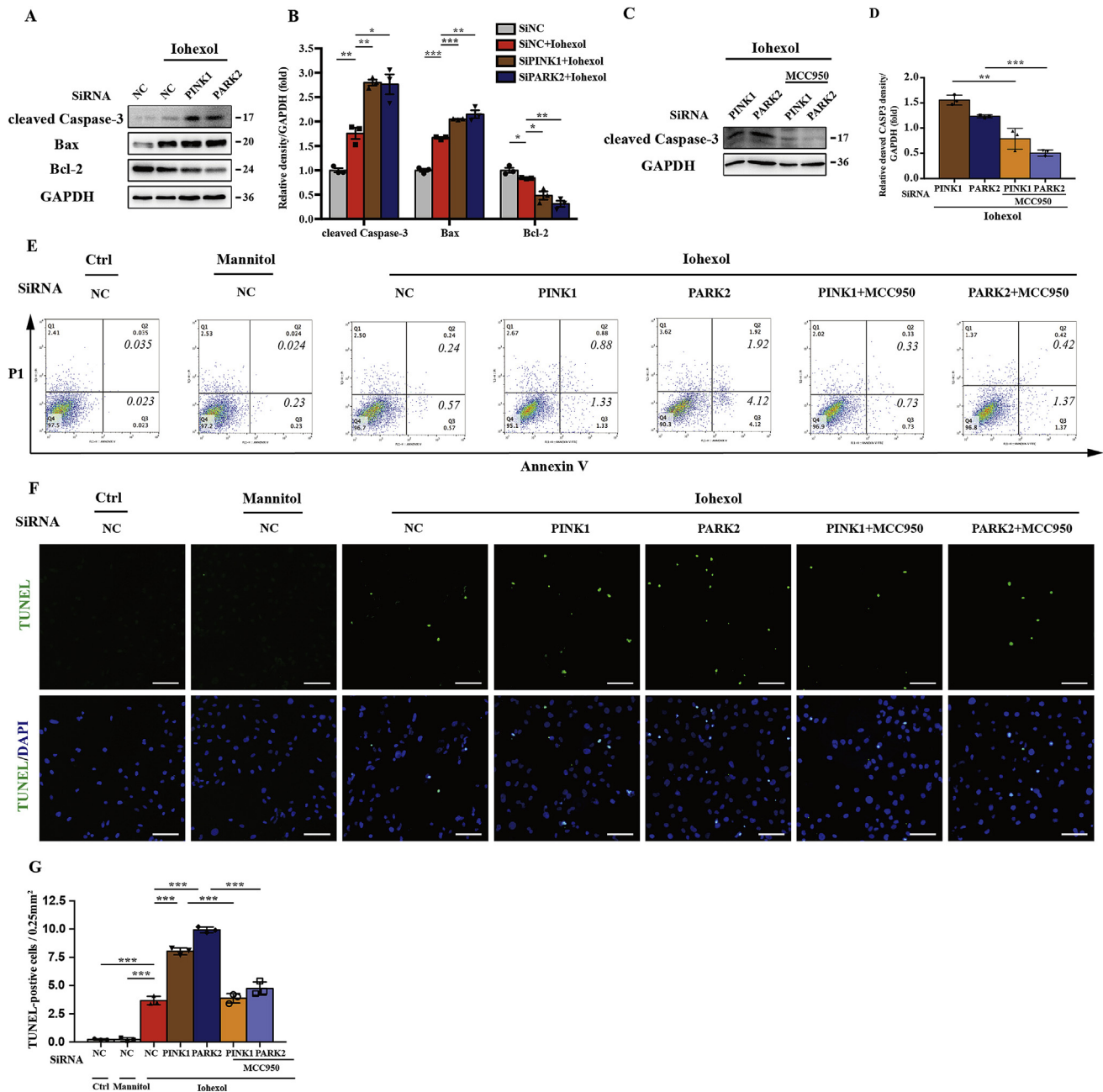


Fig. 9. Silencing PINK1 or PARK2 sensitised HK-2 cells to contrast-induced apoptosis, which was reduced by NLRP3 inflammasome inhibition. After transfection with SiNC, SiPINK1, or SiPARK2 for 8 h, HK-2 cells were pretreated with MCC950 (10 μ M) for 4 h and then cultured with iohexol for 72 h. (A, B) Immunoblot analysis and quantification of cleaved caspase-3, Bax, and Bcl-2 in SiNC, SiPINK1, or SiPARK2 cells with iohexol. (C, D) Immunoblot analysis and quantification of cleaved caspase-3 in HK-2 cells pretreated with or without MCC950 after silencing PINK1 or PARK2 in response to iohexol. (E–G) Representative images and quantification of cell apoptosis by flow cytometry and TUNEL staining of HK-2 cells. Scale bar: 100 μ m. Data were presented as mean \pm TEM. * p < 0.05, ** p < 0.01, *** p < 0.001. (For interpretation of the references to colour in this figure legend, the reader is referred to the Web version of this article.)

cleaved caspase-3 (Fig. 9C and D). Flow cytometry also showed less Annexin V-positive HK-2 cells after MCC950 treatment (Fig. 9E). Meanwhile, TUNEL-positive HK-2 cells suggested a corresponding trend (Fig. 9F and G). Collectively, the PINK1-PARK2 pathway of mitophagy could protect HK-2 cells from apoptosis by inhibiting the NLRP3 inflammasome.

4. Discussion

The function and regulation of PINK1-Parkin-mediated mitophagy on the NLRP3 inflammasome remain unknown in kidney disease, including CI-AKI. In this study, we first showed that PINK1-

Parkin-mediated mitophagy was induced in RTECs in CI-AKI, both *in vivo* and *in vitro*. Then, we demonstrated the protective role of PINK1-Parkin-mediated mitophagy in CI-AKI by using PINK1 or PARK2 knockout mice, siRNA, and inhibitor. Furthermore, we elucidated that a deficiency of PINK1-Parkin-mediated mitophagy increased mitochondrial ROS production, DNA oxidative damage, and then NLRP3 inflammasome activation, contributing to RTECs apoptosis and tubular damage in CI-AKI (Fig. 10).

Our previous research revealed that contrast media activated the NLRP3 inflammasome and increased the release of downstream inflammatory cytokine IL-1 β , which induced gasdermin-D (GSDMD)-dependent pyroptosis [5,6]. However, the mechanism of

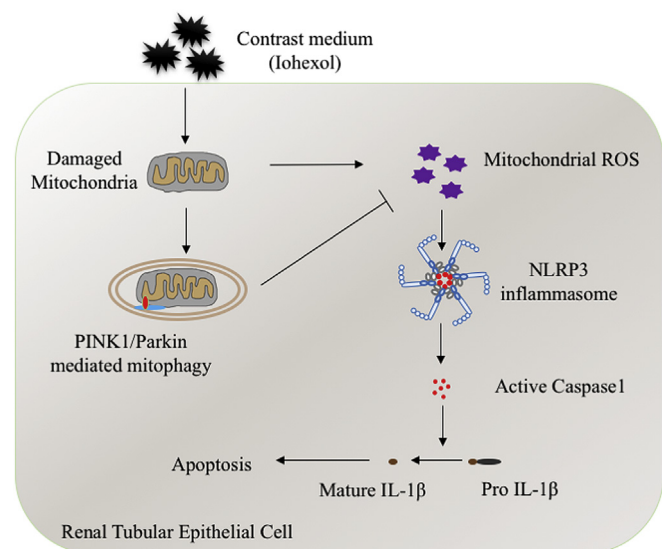


Fig. 10. Schematic representation of mitophagy, mitochondrial ROS, and NLRP3 inflammasome in CI-AKI. Contrast media (iohexol) causes the mitochondrial damage of renal tubular epithelial cells, which induces mitochondrial ROS and NLRP3 inflammasome activation. PINK1-Parkin-mediated mitophagy is also activated to repair the damaged mitochondria through reducing mitochondrial ROS production and NLRP3 inflammasome activation, which decreases apoptosis of renal tubular epithelial cells and kidney injury in CI-AKI. (For interpretation of the references to colour in this figure legend, the reader is referred to the Web version of this article.)

NLRP3 inflammasome activation in CI-AKI is ill-defined [22]. Other research has demonstrated that the NLRP3 inflammasome can be activated by ROS and subsequent DNA oxidative damage in macrophages and human corneal epithelial cells [27,30]. In this study, we demonstrated that, *in vivo* and *in vitro*, contrast media activated mitochondrial ROS production, subsequent DNA oxidative damage, and the NLRP3 inflammasome (Fig. 3F-H, 8A-8D). MitoTEMPO, mitochondrial targeted antioxidant, decreased NLRP3 inflammasome activation through reduction of mitochondrial ROS and 8-OHdG (Fig. 8G-J), indicating that mitochondrial ROS and oxidised DNA are the triggers of the NLRP3 inflammasome in CI-AKI.

Recently, many research studies have focused on mitophagy and the NLRP3 inflammasome. In macrophage research, Zhong et al. suggested that NF- κ B restrained its own NLRP3 inflammasome activation through the NF- κ B-p62 mitophagy pathway [31]. The NLRP3 inflammasome activated in sepsis or myocardial mitochondrial stress was also eliminated by mitophagy [32–34]. In kidney research, Chen and colleagues demonstrated that optineurin induced mitophagy to inhibit the activation of NLRP3 in DKD [25]. Xu et al. showed that prohibitin 2-induced mitophagy inhibited the NLRP3 inflammasome in CKD, through amelioration of mitochondrial dysfunction [35]. Here, we demonstrated that PINK1-Parkin-mediated mitophagy played a crucial role in the NLRP3 inflammasome in AKI research. When exposed to contrast media, a deficiency of PINK1 or PARK2 decreased the activity of MnSOD (Fig. 3F, 8D) and increased mitochondrial ROS production (Fig. 8A) and NLRP3 inflammasome activation (Fig. 3I, 3K, 6E, 8E, 8G). Accordingly, we proposed the mitophagy-mitochondrial ROS-NLRP3 inflammasome pathway in CI-AKI. However, other studies have had different opinions. Kim and colleagues indicated that deletion of inflammasome-independent NLRP3 induced mitophagy and clearance of mitochondrial ROS in unilateral ureter obstruction model [36]. Meanwhile, Yu et al. demonstrated that caspase-1 knockout increased mitophagy and reduced mitochondrial damage in macrophages, indicating caspase-1 mediated Parkin cleavage [37]. Thus, it would be interesting to investigate further the effect of the NLRP3 inflammasome on mitophagy and mitochondrial dysfunction, as well as the cross-talk between

the NLRP3 inflammasome and mitophagy.

In the past few years, the function of mitophagy has been discussed in kidney diseases. The reduction of mitophagy in DKD models could be rescued by the mitochondria-targeted antioxidants optineurin and forkhead-box class O1 (FOXO1) to protect RTECs, podocytes, and M1/M2 macrophage phenotype [17,38–40]. PINK-Parkin-mediated mitophagy is demonstrated to prevent cisplatin-induced RTECs apoptosis and tissue damage *in vitro* and *in vivo* [19,20]. Two main pathways of mitophagy, PINK1-Parkin-mediated and BNIP3-mediated, were demonstrated to alleviate mitochondrial damage and protect renal tubules in renal ischemia-reperfusion injury [18,41]. A few research studies have shown the protective effect of mitophagy on apoptosis of RTECs in a cell or rat model of CI-AKI [21–23]. However, the specific pathway of mitophagy and the mechanism of mitophagy on apoptosis have still been unclear in CI-AKI. In this study, we first verified the PINK1-Parkin pathway in CI-AKI (Fig. 2A, 5G-J) and then elucidated the protective role of PINK1-Parkin-mediated mitophagy by 3-MA, PINK1, or PARK2 knockout mice and siRNA (Fig. 2H-K, 6G, 7C-F, 9A). Next, we showed that RTECs apoptosis was reduced through decreased mitochondrial ROS production, subsequent DNA oxidative damage, and NLRP3 inflammasome by using MitoTEMPO and MCC950 (Fig. 4, 8G-J, 9). Nowadays, the debate remains unsettled between autophagic cell death and cell death accompanied by autophagy [42], and our results supported the latter in CI-AKI. Although both RTECs apoptosis and mitophagy (being a form of autophagy) increased after iohexol treatment, deficiency of PINK1-Parkin-mediated mitophagy caused more RTEC apoptosis in CI-AKI, indicating that mitophagy was protective for apoptosis of RTECs.

Most studies reached a conclusion that was consistent with ours, as PINK1 regulated Parkin to mediate mitophagy in mammals [43,44]. Interestingly, many research studies have demonstrated that PINK1 and Parkin had functions other than mediating mitophagy, especially in immunity [45]. Parkin had roles in innate immunity by promoting ubiquitin-mediated autophagy to degrade intracellular bacterial pathogens [46]. In adaptive immunity, PINK1 and Parkin inhibited the generation of mitochondrial-derived vesicles and mitochondrial antigen presentation, which suppressed the immune response-eliciting pathway by inflammation in Parkinson's disease [47]. Consequently, future studies should focus on the mitophagy-independent function of PINK1 and Parkin in kidney disease.

In this study, we demonstrated the relationship between mitophagy, mitochondrial ROS, DNA oxidative damage, NLRP3 inflammasome, and apoptosis of RTECs. Based on our research, urine mitochondrial ROS, 8-OHdG, IL-1 β , and IL-18 levels could be considered biomarkers in monitoring the disease activity of CI-AKI in the future. In the clinical setting, the PRSERVE study has shown no benefit of oral acetylcysteine with/without intravenous sodium bicarbonate in high-risk CI-AKI patients [3]. However, the conclusions of our study indicate that mitochondrial-targeted antioxidant or mitophagy agonist could have a benefit for CI-AKI patients. We have started a study of drugs in CI-AKI animal models to validate our supposition.

In summary, we demonstrated that the PINK1-Parkin pathway of mitophagy was induced in CI-AKI, both *in vivo* and *in vitro*. PINK1-Parkin-mediated mitophagy prevented RTEC apoptosis and tissue damage after contrast media intervention through decreasing mitochondrial ROS and DNA oxidative damage and subsequently inhibiting the activation of the NLRP3 inflammasome. Therapeutic strategies aiming at upregulation of mitophagy may preserve mitochondrial function of tubular epithelial cells against CI-AKI.

Author contributions

Q.L. designed and performed most experiments, and wrote the manuscript. S.L. analysed the data and edited the manuscript. N.J. and X.S. helped design the animal experiments. M.Z. and Z.Z. analysed the histology and histopathology. H.J. helped edit the manuscript. J.S., Y.Z.

and W.Z. helped design cell experiments and interpret data. L.G. and R.L. helped interpret data. Z.N. supervised all experiments, and edited the manuscript.

Conflicts of interest

The authors declare that they have no conflict of interest.

Acknowledgments

This study was supported by grants from National Natural Science Foundation of China (81770666, 81570604, 81370794), Shanghai Municipal Health Commission Project (ZY (2018–2020)-FWTX-1001), National Basic Research Program of China 973 Program (2012CB517602) to Z.N. and National Natural Science Foundation of China (81700586) for J.S.

Appendix A. Supplementary data

Supplementary data to this article can be found online at <https://doi.org/10.1016/j.redox.2019.101254>.

Abbreviation

3-MA	3-Methyladenine
8-OHdG	8-hydroxy-2 deoxyguanosine
AKI	acute kidney injury
B2M	beta-2 microglobulin
Bax	BCL-2 Associated X Protein
Bcl-2	B-cell lymphoma 2
BNIP3	BCL-2 and adenovirus E1B 19-kDa-interacting protein3
BNIP3L	BNIP3-like
CI-AKI	Contrast-induced acute kidney injury
CKD	chronic kidney disease
COX IV	cytochrome c oxidase subunit 4I1
Ctrl	control
Cyto c	cytochrome C
DAMPs	damage-associated molecular patterns
DAPI	40,6-Diamidino-2-phenylindole dihydrochloride
DKD	diabetic kidney disease
DRP1	dynamain-related protein 1
GAPDH	glyceraldehyde-3-phosphate dehydrogenase
GSDMD	gasdermin-D
H ₂ O ₂	hydrogen peroxide
HE	haematoxylin and eosin
HRP	horseradish peroxidase
IL-18	interleukin 18
IL-1β	interleukin 1 beta
KIM-1	kidney injury molecule-1
MAP1LC3B/LC3B	microtubule-associated protein 1 light chain 3 beta
MFN1	mitofusin1
MnSOD	manganese-dependent superoxide dismutase, SOD2
mRNA	messenger RNA
mtDNA	mitochondrial DNA
MT-ND1	mitochondrial NADH-ubiquinone oxidoreductase chain 1
nDNA	nuclear DNA
NF-κB	Nuclear factor κB
NLRP3	Nucleotide-binding oligomerisation domain-like pyrin domain containing protein 3
NS	natural saline
PAMPs	pathogen-associated molecular patterns
PARK2	parkin RBR E3 ubiquitin protein ligase, Parkinson disease 2
PFA	paraformaldehyde
PI	propidine iodid
PINK1	PTEN induced putative kinase 1
PRR	pattern recognition receptors

RIPA	Radio-Immunoprecipitation Assay
ROS	reactive oxygen species
RTEC	renal tubular epithelial cell
SEM	standard error of the mean
siRNA	small interfering RNA
SQSTM1	sequestosome 1
TEM	transmission electron microscopy
TOM	outer mitochondrial membrane
TUNEL	terminal deoxynucleotidyl transferase mediated dUTP nick end labeling
VDAC	Voltage-dependent anion channel
WST-8	2-(2-methoxy-4-nitrophenyl)-3-(4-nitrophenyl)-5-(2,4-disulfophenyl)-2H-tetrazolium, monosodium salt-8
WT	wild-type

References

- [1] M. Fahling, E. Seeliger, A. Patzak, et al., Understanding and preventing contrast-induced acute kidney injury, *Nat. Rev. Nephrol.* 13 (3) (2017) 169–180.
- [2] A. Khwaja, KDIGO clinical practice guidelines for acute kidney injury, *Nephron Clin. Pract.* 120 (4) (2012) c179–c184.
- [3] S.D. Weisbord, M. Gallagher, H. Jneid, et al., Outcomes after angiography with sodium bicarbonate and acetylcysteine, *N. Engl. J. Med.* 378 (7) (2018) 603–614.
- [4] T. Scharnweber, L. Alhilali, S. Fakhran, Contrast-induced acute kidney injury: pathophysiology, manifestations, prevention, and management. *Magn reson imaging, Clin N Am* 25 (4) (2017) 743–753.
- [5] J. Shen, L. Wang, N. Jiang, et al., NLRP3 inflammasome mediates contrast media-induced acute kidney injury by regulating cell apoptosis, *Sci. Rep.* (2016) 634682.
- [6] Z. Zhang, X. Shao, N. Jiang, et al., Caspase-11-mediated tubular epithelial pyroptosis underlies contrast-induced acute kidney injury, *Cell Death Dis.* 9 (10) (2018) 983.
- [7] A. Lau, H. Chung, T. Komada, et al., Renal immune surveillance and dipeptidase-1 contribute to contrast-induced acute kidney injury, *J. Clin. Investig.* 128 (7) (2018) 2894–2913.
- [8] M. Yabal, D.J. Calleja, D.S. Simpson, et al., Stressing out the mitochondria: mechanistic insights into NLRP3 inflammasome activation, *J. Leukoc. Biol.* 105 (2) (2018) 377–399.
- [9] C. Juliana, T. Fernandes-Alnemri, S. Kang, et al., Non-transcriptional priming and deubiquitination regulate NLRP3 inflammasome activation, *J. Biol. Chem.* 287 (43) (2012) 36617–36622.
- [10] B. Levine, G. Kroemer, Biological functions of autophagy genes: a disease perspective, *Cell* 176 (1–2) (2019) 11–42.
- [11] A. Angajala, S. Lim, J.B. Phillips, et al., Diverse roles of mitochondria in immune responses: novel insights into immuno-metabolism, *Front. Immunol.* (2018) 91605.
- [12] R.J. Youle, D.P. Narendra, Mechanisms of mitophagy, *Nat. Rev. Mol. Cell Biol.* 12 (1) (2011) 9–14.
- [13] M. Bueno, Y.C. Lai, Y. Romero, et al., PINK1 deficiency impairs mitochondrial homeostasis and promotes lung fibrosis, *J. Clin. Investig.* 125 (2) (2015) 521–538.
- [14] M. Zimmermann, A.S. Reichert, How to get rid of mitochondria: crosstalk and regulation of multiple mitophagy pathways, *Biol. Chem.* 399 (1) (2017) 29–45.
- [15] M.N. Quinsay, R.L. Thomas, Y. Lee, et al., Bnip3-mediated mitochondrial autophagy is independent of the mitochondrial permeability transition pore, *Autophagy* 6 (7) (2010) 855–862.
- [16] Y. Yuan, Y. Zheng, X. Zhang, et al., BNIP3L/NIX-mediated mitophagy protects against ischemic brain injury independent of PARK2, *Autophagy* 13 (10) (2017) 1754–1766.
- [17] L. Xiao, X. Xu, F. Zhang, et al., The mitochondria-targeted antioxidant MitoQ ameliorated tubular injury mediated by mitophagy in diabetic kidney disease via Nrf2/PINK1, *Redox Biol* (2017) 11297–11311.
- [18] C. Tang, H. Han, M. Yan, et al., PINK1-PRKN/PARK2 pathway of mitophagy is activated to protect against renal ischemia-reperfusion injury, *Autophagy* 14 (5) (2018) 880–897.
- [19] C. Zhao, Z. Chen, X. Xu, et al., Pink1/Parkin-mediated mitophagy play a protective role in cisplatin induced renal tubular epithelial cells injury, *Exp. Cell Res.* 350 (2) (2017) 390–397.
- [20] Y. Wang, C. Tang, J. Cai, et al., PINK1/Parkin-mediated mitophagy is activated in cisplatin nephrotoxicity to protect against kidney injury, *Cell Death Dis.* 9 (11) (2018) 1113.
- [21] X. Yang, X. Yan, D. Yang, et al., Rapamycin attenuates mitochondrial injury and renal tubular cell apoptosis in experimental contrast-induced acute kidney injury in rats, *Biosci. Rep.* 38 (6) (2018).
- [22] W. Cheng, F. Zhao, C.Y. Tang, et al., Comparison of iohexol and iodixanol induced nephrotoxicity, mitochondrial damage and mitophagy in a new contrast-induced acute kidney injury rat model, *Arch. Toxicol.* 92 (7) (2018) 2245–2257.
- [23] R. Lei, F. Zhao, C.Y. Tang, et al., Mitophagy plays a protective role in iodinated contrast-induced acute renal tubular epithelial cells injury, *Cell. Physiol. Biochem.* 46 (3) (2018) 975–985.
- [24] X. Guan, Y. Qian, Y. Shen, et al., Autophagy protects renal tubular cells against ischemia/reperfusion injury in a time-dependent manner, *Cell. Physiol. Biochem.* 36 (1) (2015) 285–298.

- [25] K. Chen, L. Feng, W. Hu, et al., Optineurin inhibits NLRP3 inflammasome activation by enhancing mitophagy of renal tubular cells in diabetic nephropathy, *FASEB J.* 33 (3) (2018) 4571–4585.
- [26] W. Song, L. Wei, Y. Du, et al., Protective effect of ginsenoside metabolite compound K against diabetic nephropathy by inhibiting NLRP3 inflammasome activation and NF-kappaB/p38 signaling pathway in high-fat diet/streptozotocin-induced diabetic mice, *Int. Immunopharmacol.* (2018) 63227–63238.
- [27] W. Chi, X. Hua, X. Chen, et al., Mitochondrial DNA oxidation induces imbalanced activity of NLRP3/NLRP6 inflammasomes by activation of caspase-8 and BRCC36 in dry eye, *J. Autoimmun.* (2017) 8065–8076.
- [28] Q. Wu, X. Ni, ROS-mediated DNA methylation pattern alterations in carcinogenesis, *Curr. Drug Targets* 16 (1) (2015) 13–19.
- [29] A. Pour Khavari, Y. Liu, E. He, et al., Serum 8-Oxo-dG as a predictor of sensitivity and outcome of radiotherapy and chemotherapy of upper gastrointestinal tumours, *Oxid Med Cell Longev* (2018) 4153574.
- [30] Z. Zhong, S. Liang, E. Sanchez-Lopez, et al., New mitochondrial DNA synthesis enables NLRP3 inflammasome activation, *Nature* 560 (7717) (2018) 198–203.
- [31] Z. Zhong, A. Umemura, E. Sanchez-Lopez, et al., NF-kappaB restricts inflammasome activation via elimination of damaged mitochondria, *Cell* 164 (5) (2016) 896–910.
- [32] R. Kang, L. Zeng, Y. Xie, et al., A novel PINK1- and PARK2-dependent protective neuroimmune pathway in lethal sepsis, *Autophagy* 12 (12) (2016) 2374–2385.
- [33] M.J. Kim, S.H. Bae, J.C. Ryu, et al., SESN2/sestrin2 suppresses sepsis by inducing mitophagy and inhibiting NLRP3 activation in macrophages, *Autophagy* 12 (8) (2016) 1272–1291.
- [34] H. Li, W. Miao, J. Ma, et al., Acute exercise-induced mitochondrial stress triggers an inflammatory response in the myocardium via NLRP3 inflammasome activation with mitophagy, *Oxid Med Cell Longev* (2016) 1987149.
- [35] Y. Xu, J. Wang, W. Xu, et al., Prohibitin 2-mediated mitophagy attenuates renal tubular epithelial cells injury by regulating mitochondrial dysfunction and NLRP3 inflammasome activation, *Am. J. Physiol. Renal. Physiol.* 316 (2) (2018) F396–F407.
- [36] S.M. Kim, Y.G. Kim, D.J. Kim, et al., Inflammasome-independent role of NLRP3 mediates mitochondrial regulation in renal injury, *Front. Immunol.* (2018) 92563.
- [37] J. Yu, H. Nagasu, T. Murakami, et al., Inflammasome activation leads to Caspase-1-dependent mitochondrial damage and block of mitophagy, *Proc. Natl. Acad. Sci. U. S. A.* 111 (43) (2014) 15514–15519.
- [38] K. Chen, H. Dai, J. Yuan, et al., Optineurin-mediated mitophagy protects renal tubular epithelial cells against accelerated senescence in diabetic nephropathy, *Cell Death Dis.* 9 (2) (2018) 105–112.
- [39] W. Li, M. Du, Q. Wang, et al., FoxO1 promotes mitophagy in the podocytes of diabetic male mice via the PINK1/parkin pathway, *Endocrinology* 158 (7) (2017) 2155–2167.
- [40] Y. Zhao, Y. Guo, Y. Jiang, et al., Mitophagy regulates macrophage phenotype in diabetic nephropathy rats, *Biochem. Biophys. Res. Commun.* 494 (1–2) (2017) 42–50.
- [41] M. Ishihara, M. Urushido, K. Hamada, et al., Sestrin-2 and BNIP3 regulate autophagy and mitophagy in renal tubular cells in acute kidney injury, *Am. J. Physiol. Renal. Physiol.* 305 (4) (2013) F495–F509.
- [42] J. Doherty, E.H. Baehrecke, Life, death and autophagy, *Nat. Cell Biol.* 20 (10) (2018) 1110–1117.
- [43] D.A. Sliter, J. Martinez, L. Hao, et al., Parkin and PINK1 mitigate STING-induced inflammation, *Nature* 561 (7722) (2018) 258–262.
- [44] T.N. Nguyen, B.S. Padman, M. Lazarou, Deciphering the molecular signals of PINK1/parkin mitophagy, *Trends Cell Biol.* 26 (10) (2016) 733–744.
- [45] L.A. Scarffe, D.A. Stevens, V.L. Dawson, et al., Parkin and PINK1: much more than mitophagy, *Trends Neurosci.* 37 (6) (2014) 315–324.
- [46] P.S. Manzanillo, J.S. Ayres, R.O. Watson, et al., The ubiquitin ligase parkin mediates resistance to intracellular pathogens, *Nature* 501 (7468) (2013) 512–516.
- [47] D. Matheoud, A. Sugiura, A. Bellemare-Pelletier, et al., Parkinson's disease-related proteins PINK1 and parkin repress mitochondrial antigen presentation, *Cell* 166 (2) (2016) 314–327.